HHS Public Access

Author manuscript

J Am Chem Soc. Author manuscript; available in PMC 2023 June 02.

Published in final edited form as:

J Am Chem Soc. 2023 January 18; 145(2): 1097–1107. doi:10.1021/jacs.2c10666.

Ultrasound-Triggered In Situ Photon Emission for Noninvasive Optogenetics

Wenliang Wang[‖],
Biomedical Engineering Cockrell School of Engineering, The University of Texas at Austin, Austin, Texas 78712, United States

Xiang Wu[‖],
Department of Materials Science and Engineering, Stanford University, Stanford, California 94305, United States; Wu Tsai Neurosciences Institute, Stanford University, Stanford, California 94305, United States

Kai Wing Kevin Tang[‖],
Biomedical Engineering Cockrell School of Engineering, The University of Texas at Austin, Austin, Texas 78712, United States

Ilya Pyatnitskiy,
Biomedical Engineering Cockrell School of Engineering, The University of Texas at Austin, Austin, Texas 78712, United States

Rayna Taniguchi,
Biomedical Engineering Cockrell School of Engineering, The University of Texas at Austin, Austin, Texas 78712, United States

Peter Lin,
Biomedical Engineering Cockrell School of Engineering, The University of Texas at Austin, Austin, Texas 78712, United States

Richard Zhou,

Corresponding Authors: **Guosong Hong** – *Department of Materials Science and Engineering, Stanford University, Stanford, California 94305, United States; Wu Tsai Neurosciences Institute, Stanford University, Stanford, California 94305, United States;* guosongh@stanford.edu; **Huiliang Wang** – *Biomedical Engineering Cockrell School of Engineering, The University of Texas at Austin, Austin, Texas 78712, United States;* evanwang@utexas.edu.

[‖]Author Contributions

W.W., X.W., and K.W.K.T. contributed equally to this work.

Supporting Information

The Supporting Information is available free of charge at https://pubs.acs.org/doi/10.1021/jacs.2c10666.

Light emission from Lipo@IR780/L012 through a photon processing system in real time (MP4)

Red fluorescence enhancement as a result of binding of calcium ion (Ca^{2+}) indicators with pGP-CMV-NES-jRGECO1a plasmids in spiking HEK cells (MP4)

Camera video tracking the synchronized limbs' response under the sono-optogenetic stimulations, where the hip, knee, and feet are marked with different colored dots (MP4)

Synthesis and characterization of the FUS peak pressure, histology tests, additional fluorescence images, Deep-LabCut framework in extracting kinematics data, time-resolved limbs' hip–knee and knee–feet response, ROS detection, and characterization of blue light emission from nanoparticles (PDF)

Complete contact information is available at: https://pubs.acs.org/doi/10.1021/jacs.2c10666

The authors declare the following competing financial interest(s): The authors declare that a patent application relating to this work has been filed.

Biomedical Engineering Cockrell School of Engineering, The University of Texas at Austin, Austin, Texas 78712, United States

Sam Lander C. Capocyan,
Biomedical Engineering Cockrell School of Engineering, The University of Texas at Austin, Austin, Texas 78712, United States

Guosong Hong,
Department of Materials Science and Engineering, Stanford University, Stanford, California 94305, United States; Wu Tsai Neurosciences Institute, Stanford University, Stanford, California 94305, United States

Huiliang Wang
Biomedical Engineering Cockrell School of Engineering, The University of Texas at Austin, Austin, Texas 78712, United States

Abstract

Optogenetics has revolutionized neuroscience understanding by allowing spatiotemporal control over cell-type specific neurons in neural circuits. However, the sluggish development of noninvasive photon delivery in the brain has limited the clinical application of optogenetics. Focused ultrasound (FUS)-derived mechanoluminescence has emerged as a promising tool for in situ photon emission, but there is not yet a biocompatible liquid-phase mechanoluminescence system for spatiotemporal optogenetics. To achieve noninvasive optogenetics with a high temporal resolution and desirable biocompatibility, we have developed liposome (Lipo@IR780/L012) nanoparticles for FUS-triggered mechanoluminescence in brain photon delivery. Synchronized and stable blue light emission was generated in solution under FUS irradiation due to the cascade reactions in liposomes. In vitro tests revealed that Lipo@IR780/L012 could be triggered by FUS for light emission at different stimulation frequencies, resulting in activation of opsin-expressing spiking HEK cells under the FUS irradiation. In vivo optogrnetic stimulation further demonstrated that motor cortex neurons could be noninvasively and reversibly activated under the repetitive FUS irradiation after intravenous injection of lipid nanoparticles to achieve limb movements.

Graphical Abstract

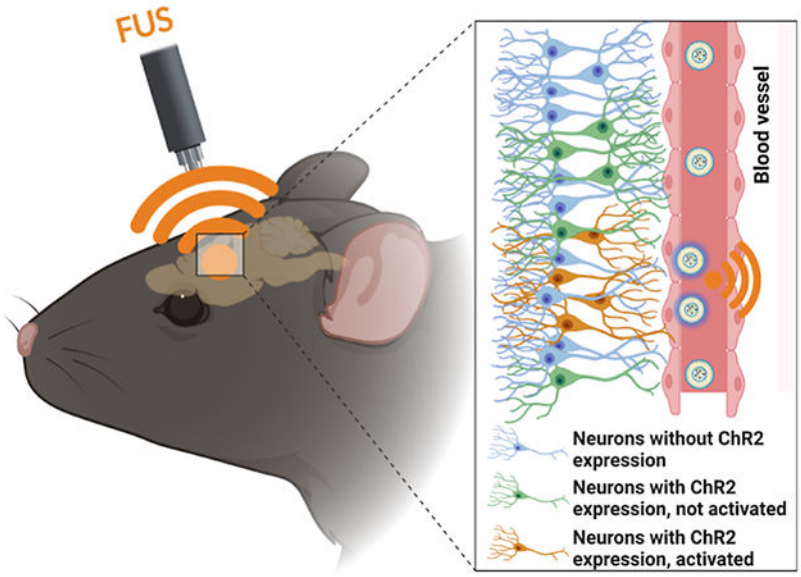

INTRODUCTION

Over the past decade, optogenetics has become an increasingly important technology for neuroscience research and the treatment of neurological disorders, including Parkinson's disease (PD) and Alzheimer's disease (AD), by providing neuroscientists with precise spatiotemporal control of neural activity with neuron subtype specificity.[1–3] However, since visible light has limited penetration in tissues, invasive partial scalp removal and implantation of optical fibers are usually required for in vivo optogenetic stimulation, resulting in permanent damage and chronic gliosis in the brain tissue.[1] In addition, perturbation of glial and astrocytic activity and ischemia have been reported during optogenetics due to the intracranial implantation of the device.[4,5] To achieve biocompatible optogenetics, several less invasive strategies have been developed such as two-photon stimulation[6] or upconversion of nanoparticles to convert tissue-penetrating near-infrared (NIR) light into visible light after intracortical injection.[7] However, the slight improvements in penetration depth using red or NIR light is still insufficient for noninvasive deep brain optogenetic stimulation, especially for large animals and human applications. On the other hand, novel opsins with higher light sensitivity have also been designed to achieve noninvasive brain stimulation up to a depth of 5–10 mm, such as ChRmine opsins with red-shifted activation spectra[8,9] and step function opsin with ultra-high light sensitivity (SOUL).[10,11] Despite these advances, it is most desirable to develop energy modality for an even higher tissue penetration for potential use in large animal or human.

Focused ultrasound (FUS) represents one form of a wireless energy harvesting strategy that has been recently developed for noninvasive local brain anesthesia, sonodynamic therapy, and chemogenetics for brain stimulation due to its superior tissue penetration depth exceeding 10 cm and biosafety.[12–15] While FUS was experiencing rapid development for biomedical applications, ultrasound-triggered noninvasive optogenetics was still in

its infancy due to the limited progress in mechanoluminescence materials.[16] Recently, we developed inorganic zinc sulfide nanoparticles co-doped with silver and cobalt (ZnS/Ag,Co@ZnS) to convert ultrasound wave to light for optogenetic stimulation.[17,18] However, ZnS/Ag,Co@ZnS nanoparticles required charging with 400 nm light outside the brain before use, and these non-biodegradable inorganic nanoparticles may generally undergo bioaccumulation and bioaugmentation of heavy metals in organs.[19–21] It is desirable to develop more biocompatible organic materials as mechanoluminescent materials for sono-optogenetics. Generally, ultrasound-induced piezoelectric effects and cycloreversions dominated the development of mechanoluminescent organic materials.[16] One example would be dioxetane crosslinked solid polymers to achieve FUS-derived blue light emission due to the cycloreversions under high intensity ultrasound stimulation.[17] While all of these mechanoluminescent materials can produce light emission in the bulk form,[16] there is not yet a biocompatible liquid-phase mechanoluminescent materials system for non-invasive sono-optogenetics. To uncover the potential of mechanoluminescence in noninvasive brain stimulation, it is necessary to develop other mechanoluminescent materials to extend the toolbox of ultrasound-induced mechanophores.[20–22]

Attributed to its natural constituents, lipids are effectively metabolized in the body. They were the first nanodrugs in FDA clinical trials and have been extensively applied in nanomedicines since the first liposomal formulation was approved by the FDA in mid-1990s.[23–25] More recently, the lipids-based mRNA vaccine developed by BioNTech/Pfizer and Moderna was clinically applied against COVID-19.[26] In this work, we designed an organic nanoparticle light source based on liposomes for noninvasive deep brain optogenetic stimulation under FUS. This nanoscopic light source comprises three primary constituents: chemiluminescent compound L012, sonosensitizer IR780, and a lipid vehicle. L012 and IR780 are loaded into the lipids to act as nanoscopic light sources due to the FUS-derived cascade reactions. Specifically, sonosensitizer IR780 generates free radicals by transferring ultrasound energy to nearby oxygen or water molecules through acoustic cavitation.[12,27] The chemiluminescent L012 is then activated by free radicals, producing light, which can be used for activating opsins expressed by specific types of neurons for controlling animal behaviors or treating diseases in the future (Scheme 1).

RESULTS AND DISCUSSION

To prepare the FUS-triggered nanoscopic light source, liposomes were first prepared. The unilamellar vesicles (Figure S1a) were prepared through a thin film hydration strategy.[28] Then, L012 and IR780 were loaded into the vehicles to fabricate the FUS-triggered nano light source (Lipo@IR780/L012) (Figure 1a). IR780-loaded liposomes (Lipo@IR780) exhibited negligible size differences compared with blank liposomes, as shown in Figure 1b and Table 1. Transmission electron microscopy (TEM) showed a uniform spherical shape of Lipo@IR780/L012 (Figure 1c) compared with the typical liposome morphology of blank lipid vehicles (Figure S1a) due to the integration of IR780/L012, where hydrophobic IR780 was inserted into the liposome membrane walls with smaller aggregates. We evaluated the stability of Lipo@IR780/L012 nanoparticles via dynamical light scattering (DLS) in a body fluid mimic solution and FUS irradiation. There were no obvious size changes after incubation in a 10% fetal bovine serum (FBS)-containing solution or FUS irradiation

(Figure 1d). In addition, there was no obvious leakage of loading cargoes from nanoparticles under the FUS stimulation (Figure S1e). These results indicated the excellent stability of Lipo@IR780/L012 nanoparticles in simulated blood fluid under FUS. The drug loading content (DLC) values of IR780 (~4.6 wt %) and L012 (~4.3 wt %) were measured from the UV–vis spectrum according to the calibration curves (Figure S1b,c), and the efficient drug loading capacity of the lipid vehicles was indicated. The Lipo@IR780/L012 nanoparticles with an average diameter of about 120 nm (Figure 1b,d and Table 1) and a negative surface zeta potential (Figure S1d and Table 1) were good for circumventing rapid clearance via the reticuloendothelial system, liver, and kidney after intravenous (i.v.) administration.[29,30]

Sonosensitizer IR780 has been reported to generate reactive oxygen species (ROS) under FUS stimulation due to acoustic cavitation and has been extensively developed for the cancer sonodynamic therapy.[12,27,31,32] In fact, the singlet oxygen ($^1O_2$) and hydroxyl radical ($^{\cdot}OH$) are the main species of ROS generated in sonochemistry.[33,34] As the primary trigger of the Lipo@IR780/L012 nano light source, ROS are crucial in activating the system through a rapid reaction with L012. Thus, we first investigated the types of generated ROS in Lipo@IR780 nanoparticles. 1,3-Diphenylisobenzofuran (DPBF) and salicylic acid (SA) probes were adopted to specifically detect the generation of $^1O_2$ and $^{\cdot}OH$ under FUS irradiation (Figure 2a). DPBF possesses highly specific reactivity toward $^1O_2$, forming 1,2-dibenzoylbenzene (DBB) as shown in Figure 2a(i).[35–37] The Lipo@IR780-containing DPBF solution was irradiated under different durations of FUS (1.5 MHz, 1.5 MPa). As shown in Figure 2b, the characteristic UV–vis absorption peak of DPBF at 420 nm dramatically decreased with the extension of FUS time due to the decomposition of DPBF in the presence of $^1O_2$, while no obvious changes were seen without FUS irradiation (Figure S2a). The quantification determined that around 52% DPBF was decomposed after 60 s of FUS irradiation, but there was no DPBF consumption without FUS irradiation (Figure 2c). Notably, the generation of $^1O_2$ was an FUS power-dependent process, which was positively related to FUS peak pressure (Figure S2b) when peak pressure was above 0.4 MPa (no $^1O_2$ generation below 0.4 MPa). Similarly, SA was used to track the generation of $^{\cdot}OH$ from Lipo@IR780. SA specifically scavenges $^{\cdot}OH$ to form 2,3-dihidroxybenzoic acid and 2,5-dihydroxibenzoic acid (Figure 2a(ii) and 2d–e). We did not observe obvious UV–vis spectral intensity changes of Lipo@IR780 at 297 nm without FUS irradiation (Figures 2f and S2c). However, the UV–vis spectral intensity at 297 nm gradually decreased with the FUS irradiation time due to the decomposition of SA, and around 36% of SA reacted with $^{\cdot}OH$ after 60 s of irradiation (Figure 2f). In addition, the generation of $^{\cdot}OH$ was also linearly dependent on FUS peak pressure (Figure S2d). Although the ROS plays essential roles in various biological processes, it would directly kill cells by oxidation at high levels.[38,39] Thus, we further evaluated the concentrations of $^{\cdot}OH$ and $^1O_2$ after liposome encapsulation in Lipo@IR780/L012. The results showed that there were no ROS residues under FUS irradiation in Lipo@IR780/L012 (Figures 2f–g, and S2e-f) since the generated ROS were rapidly consumed by L012 to emit blue light.

Next, we investigated the mechanoluminescence performance of the Lipo@IR780/L012 system. The mechanoluminescence spectra of Lipo@IR780/L012 showed that the maximal emission peak was around 470 nm (Figure 3a), which highly overlaps with the channelrhodopsin-2 (ChR2) absorption spectrum and suggests that Lipo@IR780/L012 is

suitable to activate ChR2 for optogenetic stimulation.[40] We also detected the light emission from Lipo@IR780/L012 through a photon processing system in real time (Figure 3b and Movie S1). Time-resolved mechanoluminescence intensity revealed that a sharply increased photon density was detected upon FUS irradiation (1.5 MHz, pulse 100 ms on 900 ms off, 1.5 MPa) from the baseline of Lipo@IR780/L012 nanoparticles (Figure 3c), where the ultrasound peak pressure was calculated via amplitude calibration (Figure S3). Of note, the photon density was positively and linearly correlated with peak pressure, and no photons were detected when peak pressure was below 0.51 MPa (Figures 3d and S4), which is consistent with the FUS peak pressure-dependent ROS generation process of Lipo@IR780/L012 nanoparticles (Figure S2b,d). This shows that the rate-determining step of light emission from Lipo@IR780/L012 nanoparticles was ROS concentration since the light emission intensity exhibited a positive relation with FUS peak pressure. A high temporal resolution of light emission upon FUS irradiation is important for achieving precise control over specific neuronal activity through sono-optogenetics. Therefore, we further evaluated the FUS-triggered photon emission at different irradiation frequencies (1.5 MHz, 1.5 MPa) (Figure S5). The system could still exhibit high synchronism at 8 Hz irradiation, and there were no photon density changes with the irradiation frequencies (Figures 3e and S5). We also changed the irradiation pulses from 100 to 1000 ms, and the nanoparticles showed excellent stability to output photons and there were no influences on light intensity (Figures 3f and S6). Next, we evaluated the noninvasive activation of Lipo@IR780/L012 nanoparticles using pork skin to mimic the normal brain tissue. As shown in Figures 3g and S7, a remarkable emitted light intensity was achieved from Lipo@IR780/L012 nanoparticles even at a tissue depth around 10 mm. Specifically, the light intensity only decreased around 30% (Figure 3h) at a depth of 10 mm compared with that of the no tissue covered group but reduced more significantly at a tissue depth over 15 mm due to the dissipation and scattering of ultrasound energy into the surrounding tissue.[41] Moreover, continuous and effective light emission is crucial for long-lasting optogenetics stimulation. Therefore, we also evaluated the light emission half-time of Lipo@IR780/L012 nanoparticles under FUS irradiation. As shown in Figure 3i, the decay half-time of light intensity was around 60 s (1.5 MHz, pulse 1000 ms on 1000 ms off, 1.5 MPa). The light intensity gradually decreased with irradiation time due to the continuous and irreversible consumption of L012 until it reached around 10% after 90 s irradiation. All these results demonstrate that the Lipo@IR780/L012 system demonstrated excellent reliability and synchronism for repeated, noninvasive sono-optogenetics stimulation.

In order to evaluate the activation of opsins under repetitive FUS irradiation, we utilized CheRiff-eGFP tet-on spiking human embryonic kidney 293 (HEK) cells with the constitutively expressed blue light-activated CheRiff actuator, voltage-gated sodium channel $Na_V1.5$, and inducibly (tet-on) expressed $K_{ir}2.1$. The mechanoluminescence spectra of Lipo@IR780/L012 also highly overlapped with the CheRiff opsin absorption spectra (Figure 3a).[42] The spiking HEK cells were transfected with pGP-CMV-NES-jRGECO1a plasmids to express calcium ion (Ca^{2+}) indicators, as shown in Figure 4a and Movie S2. Once the opsins channels were activated under the irradiation of blue light, calcium ions would rapidly diffuse into the cells and then bind with the jRGECO1a calcium indicators for increased red fluorescence. Our experiments confirmed that the red fluorescence signal remarkably

increased after the spiking HEK cells with Lipo@IR780/L012 nanoparticles were irradiated by ultrasound (Figure 4b). The time-resolved red fluorescence signal revealed that the sharp increment was observed only in the Lipo@IR780/L012 nanoparticles (+) group with FUS irradiation, but no changes were observed in any other control groups without ultrasound or nanoparticles (Figure 4c), which demonstrates that the spiking HEK cells only fired when the mechanoluminescence occurred. Of note, the red fluorescence signal gently decayed with the continuous irradiation due to the photobleaching of jRGECO1a calcium indicators. In addition, mechanoluminescence power would decrease with the continuous consumption of L012 under the FUS irradiation, thus influencing the spike probability. As shown in Figure 4d, the spike probability was approximately 66% under the mechanoluminescence irradiation. We then evaluated the biosafety and biocompatibility of Lipo@IR780/L012 nanoparticles. As shown in Figure 4e, the cell viability tests in HEK cells determined that there was a minimum toxicity to the cells even when the Lipo@IR780/L012 nanoparticles concentration was up to 200 μg/mL, and there was no obvious toxicity to HEK cells after FUS stimulation due to the high stability of Lipo@IR780/L012 nanoparticles and minimum ROS residue leakage from the liposomes. The hemolysis assay shown in Figure 4f also verified high biocompatibility of Lipo@IR780/L012 nanoparticles, with only around 25% hemolysis occurring at a concentration around 1000 μg/mL under the FUS stimulation.[43,44] These results indicate that the Lipo@IR780/L012 nanoparticles are safe enough for further in vivo application.

The in vitro tests demonstrated that the opsins are effectively activated under the ultrasound irradiation with Lipo@IR780/L012 nanoparticles. Following this, we asked whether the Lipo@IR780/L012 nanoparticles allowed for noninvasive optogenetic brain stimulation in ChR2-expressing mice after tail vein administration under FUS irradiation. First, we evaluated the FUS energy delivery in the mouse brain. As shown in Figure S8, the FUS focus was set to overlap with the motor cortex region (depth ~1 mm) through adjusting the water balloon, and FUS at 60% amplitude (2.45 MPa) could provide up to 1.93 MPa at focus, which is more than the pressure (1.5 MPa) needed to generate full light emission intensity of nanoparticles. In addition, we also evaluated the distribution of Lipo@IR780/L012 nanoparticles in the brain via NIR fluorescence imaging. As shown in Figure S9, the nanoparticles could be effectively delivered to the brain area and circulated in the blood after injection for 15 min, and they generated blue light under the FUS irradiation with a power intensity of 1.01 mW/mm^2 (Figure S10). Then, Thy1-ChR2-YFP transgenic mice with ChR2 expressing neurons were used for in vivo sono-optogenetic stimulation. As shown in Figure 5a, the mouse was head-fixed in a stereotaxic frame and anesthetized using 2.5% isoflurane. Then, Lipo@IR780/L012 nanoparticles at a concentration of 10 mg/mL were injected through the tail vein. The FUS transducer water balloon was placed in direct contact with the intact scalp of the mouse with filling ultrasound gel (Figure 5a). To visually evaluate sono-optogenetic brain stimulation, the motor cortex areas were irradiated (Figure 5a) since the motor cortex controls the execution of body movement, including the complex movements of the leg and fingers, allowing us to easily evaluate activation by tracking mouse movement.[45] After i.v. administration off 15 min, the isoflurane concentration was decreased to 0.5% to make sure that the mice were in the light anesthesia status in order to effectively observe its response to FUS irradiation (1.5 MHz, pulse 100 ms on 900

ms off, 2.45 MPa). A video camera was used to track the synchronized limbs' response under the sono-optogenetic stimulations, where the hip, knee, and feet were marked with different colored dots (Figure 5b and Movie S3). Kinematic data were obtained by using DeepLabCut to quantify the joint angle (hip to knee: θ and knee to feet: φ, shown in Figure 5b) changes under the ultrasound irradiation (Figure S11). Our results revealed sharp changes in θ in the Lipo@IR780/L012 nanoparticles (+) group with FUS irradiation but no change in all other groups in left and right limbs (Figures 5c–d and S12). Similar results were also observed in knee to feet movement (φ), indicating the temporary and reversible activation of motor cortex neurons under the repetitive mechanoluminescence irradiation. The quantitative analysis of θ (Figure 5e) and φ (Figure 5f) angle changes showed that there were statistically significant differences between Lipo@IR780/L012 nanoparticles (+)/FUS irradiation (+) groups and other control groups with Lipo@IR780/L012 nanoparticles (+)/FUS irradiation (−), Lipo@IR780/L012 nanoparticles(−)/FUS irradiation (+), and Lipo@IR780/L012 nanoparticles (−)/FUS irradiation (−). Previous studies have reported limb movements and auditory side effects as a result of direct, nonspecific FUS stimulation.[45–47] However, negligible limb motions were observed in our experiments when the mice were irradiated without Lipo@IR780/L012 nanoparticles, probably because the non-specific FUS stimulation depends on the anesthesia status, which is different in our studies from that in previous reports.[46–48] These results revealed that our FUS-induced Lipo@IR780/L012 system can be used to achieve highly reliable noninvasive brain stimulation. Notably, this system may be more efficient in a highly vascularized tissue where the liposomes are activated under the FUS irradiation to stimulate the neurons around the vessels. In addition, immunohistology analysis of c-fos expression, an immediate early gene and a marker of neuron activity, in the motor cortex was also conducted (Figure S13a). The results validated that the neuronal excitation could only be triggered by the presence of both FUS and Lipo@IR780/L012 nanoparticles (Figure S13b,c). Of note, lower c-fos baseline expression in the motor cortex was observed in control groups than in previous studies.[10,49–52] The reason is that we conducted the experiments in mice under anesthesia, where the neuron activity was largely suppressed under this anesthesia state. Moreover, we also evaluated the in vivo biosafety of this system by hematoxylin and eosin (H&E) staining. The mice were sacrificed, and organs (heart, liver, spleen, lung, kidney, and brain) were extracted 7 days after FUS irradiation. The results revealed there were negligible damages in these organs, suggesting excellent biosafety of our system for sono-optogenetic stimulation (Figure S14). In addition, we also evaluated the biocompatibility of this system through neuroinflammation markers Iba1 (Figure S15) and cell death marker caspase-3 (Figure S16), where these results indicated that there were no obvious glial activation and apoptosis in neuronal cells under the stimulation of this system.

CONCLUSIONS

In conclusion, we developed a biocompatible mechanoluminescence system based on organic lipid vehicles, sonosensitizer IR780, and chemiluminescent L012 to achieve noninvasive optogenetic stimulation of neural activity under FUS, without the need for charging of the nanoparticles. Ultrasound energy is noninvasively transmitted to the brain tissue and sensed via sonosensitizer IR780, generating ROS that trigger the

nearby chemiluminescent L012, resulting in blue light emission. We revealed that these Lipo@IR780/L012 nanoparticles were able to emit blue light under FUS for activating the CheRiff-expressing spiking HEK cells. Furthermore, in vivo experiments demonstrated that motor cortex neurons in Thy1-ChR2-YFP transgenic mice can be temporarily and reversibly activated under the repetitive FUS irradiation after i.v. injection of Lipo@IR780/L012, thus achieving noninvasive sono-optogenetic brain stimulation. Notably, the axial resolution of the present FUS is in the order of millimeter, and the development of FUS with a submillimeter resolution is imperative for more specific neural modulation.

Experimental Section/Methods.

The experimental details and characterization are shown in the Supporting Information. pGP-CMV-NES-jRGECO1a was a gift from the Douglas Kim & GENIE Project (Addgene plasmid # 61563; http://n2t.net/addgene:61563; RRID/Addgene_61563). CheRiff-eGFP tet-on spiking HEK cells were purchased from ATCC. Thy1-ChR2-YFP transgenic mice were ordered from Jackson laboratory. All procedures were designed according to the National Institute of Health Guide for the Care and Use of Laboratory Animals, were approved by the Institutional Animal Care and Use Committee at the University of Texas at Austin, and were supported via the Animal Resources Center at University of Texas at Austin.

Supplementary Material

Refer to Web version on PubMed Central for supplementary material.

ACKNOWLEDGMENTS

TEM image acquisition was performed with the help of Michelle Mikesh at the Center for Biomedical Research Support Microscopy and Imaging Facility at UT Austin (RRID# SCR_021756). Dr. Huiliang Wang acknowledges funding support from the NIH Mentored Research Scientist Career Development Award (National Institute of Mental Health 5K01MH117490-01), NIH Maximizing Investigators' Research Award (National Institute of General Medical Sciences 1R35GM147408), American Parkinson's Disease Association grant, Robert A. Welsh Foundation Grant (no. F-2084-20210327), University of Texas at Austin Startup Fund, UT Austin Biomedical Engineering, and UT Austin/MD Anderson Seed Grant. G.H. acknowledges two awards by NIH (5R00AG056636-04 and 1R34NS127103-01), a National Science Foundation (NSF) CAREER award (2045120), an NSF EAGER award (2217582), a Rita Allen Foundation Scholars Award, a Beckman Technology Development Grant, a grant from the Spinal Muscular Atrophy (SMA) Foundation, a grant from the Focused Ultrasound (FUS) Foundation, a gift from the Pinetops Foundation, two seed grants from the Wu Tsai Neurosciences Institute, and a seed grant from the Bio-X Initiative of Stanford University. X.W. acknowledges support from the Stanford Graduate Fellowship.

REFERENCES

(1). Deisseroth K. Optogenetics: 10 Years of Microbial Opsins in Neuroscience. Nat. Neurosci 2015, 18, 1213–1225. [PubMed: 26308982]

(2). Fougère M; van der Zouwen CI; Boutin J; Neszvecsko K; Sarret P; Ryczko D Optogenetic Stimulation of Glutamatergic Neurons in the Cuneiform Nucleus Controls Locomotion in a Mouse Model of Parkinson's Disease. Proc. Natl. Acad. Sci. U.S.A 2021, 118, No. e21109341.

(3). Etter G; van der Veldt S; Manseau F; Zarrinkoub I; Trillaud-Doppia E; Williams S Optogenetic Gamma Stimulation Rescues Memory Impairments in an Alzheimer's Disease Mouse Model. Nat. Commun 2019, 10, 5322. [PubMed: 31757962]

(4). Won SM; Song E; Reeder JT; Rogers JA Emerging Modalities and Implantable Technologies for Neuromodulation. Cell 2020, 181, 115–135. [PubMed: 32220309]

(5). Salatino JW; Ludwig KA; Kozai TDY; Purcell EK Glial Responses to Implanted Electrodes in the Brain. Nat Biomed Eng 2017, 1, 862–877. [PubMed: 30505625]

(6). Packer AM; Peterka DS; Hirtz JJ; Prakash R; Deisseroth K; Yuste R Two-Photon Optogenetics of Dendritic Spines and Neural Circuits. Nat. Methods 2012, 9, 1202–1205. [PubMed: 23142873]

(7). Chen S; Weitemier AZ; Zeng X; He L; Wang X; Tao Y; Huang AJY; Hashimotodani Y; Kano M; Iwasaki H; Parajuli LK; Okabe S; Teh DB; All AH; Tsutsui-Kimura I; Tanaka KF; Liu X; McHugh TJ Near-Infrared Deep Brain Stimulation via Upconversion Nanoparticle–mediated Optogenetics. Science 2018, 359, 679–684. [PubMed: 29439241]

(8). Marshel JH; Kim YS; Machado TA; Quirin S; Benson B; Kadmon J; Raja C; Chibukhchyan A; Ramakrishnan C; Inoue M; Shane JC; McKnight DJ; Yoshizawa S; Kato HE; Ganguli S; Deisseroth K Cortical Layer-Specific Critical Dynamics Triggering Perception. Science 2019, 365(). eaaw5202. DOI: 10.1126/science.aaw5202 [PubMed: 31320556]

(9). Chen R; Gore F; Nguyen Q-A; Ramakrishnan C; Patel S; Kim SH; Raffiee M; Kim YS; Hsueh B; Krook-Magnusson E; Soltesz I; Deisseroth K Deep Brain Optogenetics without Intracranial Surgery. Nat. Biotechnol 2020, 39, 161–164. [PubMed: 33020604]

(10). Gong X; Mendoza-Halliday D; Ting JT; Kaiser T; Sun X; Bastos AM; Wimmer RD; Guo B; Chen Q; Zhou Y; Pruner M; Wu CW-H; Park D; Deisseroth K; Barak B; Boyden ES; Miller EK; Halassa MM; Fu Z; Bi G; Desimone R; Feng G An Ultra-Sensitive Step-Function Opsin for Minimally Invasive Optogenetic Stimulation in Mice and Macaques. Neuron 2020, 107, 197. [PubMed: 32645306]

(11). Lewis S. Light Takes a Deep Dive. Nat. Rev. Neurosci 2020, 21, 349. [PubMed: 32444774]

(12). Choi V; Rajora MA; Zheng G Activating Drugs with Sound: Mechanisms Behind Sonodynamic Therapy and the Role of Nanomedicine. Bioconjug. Chem 2020, 31, 967–989. [PubMed: 32129984]

(13). Rwei AY; Paris JL; Wang B; Wang W; Axon CD; Vallet-Regí M; Langer R; Kohane DS Ultrasound-Triggered Local Anaesthesia. Nat Biomed Eng 2017, 1, 644–653. [PubMed: 29152410]

(14). Pan X; Bai L; Wang H; Wu Q; Wang H; Liu S; Xu B; Shi X; Liu H Metal-Organic-Framework-Derived Carbon Nanostructure Augmented Sonodynamic Cancer Therapy. Adv. Mater 2018, 30, 1800180.

(15). Wang JB; Aryal M; Zhong Q; Vyas DB; Airan RD Noninvasive Ultrasonic Drug Uncaging Maps Whole-Brain Functional Networks. Neuron 2018, 100, 728–738 e7. [PubMed: 30408444]

(16). Wang W; Tasset A; Pyatnitskiy I; Mohamed HG; Taniguchi R; Zhou R; Rana M; Lin P; Capocyan SLC; Bellamkonda A; Chase Sanders W; Wang H Ultrasound Triggered Organic Mechanoluminescence Materials. Adv. Drug Deliv. Rev 2022, 186, 114343. [PubMed: 35580814]

(17). Kim G; Lau VM; Halmes AJ; Oelze ML; Moore JS; Li KC High-Intensity Focused Ultrasound-Induced Mechanochemical Transduction in Synthetic Elastomers. Proc. Natl. Acad. Sci. U.S.A 2019, 116, 10214–10222. [PubMed: 31076556]

(18). Wu X; Zhu X; Chong P; Liu J; Andre LN; Ong KS; Brinson K Jr; Mahdi AI; Li J; Fenno LE; Wang H; Hong G Sono-Optogenetics Facilitated by a Circulation-Delivered Rechargeable Light Source for Minimally Invasive Optogenetics. Proc. Natl. Acad. Sci. U.S.A 2019, 116, 26332–26342. [PubMed: 31811026]

(19). Hong G. Seeing the Sound. Science 2020, 369, 638. [PubMed: 32764064]

(20). Kahlon SK; Sharma G; Julka JM; Kumar A; Sharma S; Stadler FJ Impact of Heavy Metals and Nanoparticles on Aquatic Biota. Environ. Chem. Lett 2018, 16, 919–946.

(21). Ahamed M; Akhtar MJ; Alhadlaq HA Preventive Effect of TiO2 Nanoparticles on Heavy Metal Pb-Induced Toxicity in Human Lung Epithelial (A549) Cells. Toxicol. In Vitro 2019, 57, 18–27. [PubMed: 30738203]

(22). Soenen SJ; Rivera-Gil P; Montenegro J-M; Parak WJ; De Smedt SC; Braeckmans K Cellular Toxicity of Inorganic Nanoparticles: Common Aspects and Guidelines for Improved Nanotoxicity Evaluation. Nano Today 2011, 6, 446–465.

(23). Bobo D; Robinson KJ; Islam J; Thurecht KJ; Corrie SR Nanoparticle-Based Medicines: A Review of FDA-Approved Materials and Clinical Trials to Date. Pharm. Res 2016, 33, 2373–2387. [PubMed: 27299311]

(24). Tyrrell DA; Heath TD; Colley CM; Ryman BE New Aspects of Liposomes. Biochim. Biophys. Acta 1976, 457, 259–302. [PubMed: 793635]

(25). Allen TM; Hansen CB; de Menezes DEL Pharmacokinetics of Long-Circulating Liposomes. Adv. Drug Deliv. Rev 1995, 16, 267–284.

(26). Schoenmaker L; Witzigmann D; Kulkarni JA; Verbeke R; Kersten G; Jiskoot W; Crommelin DJA mRNA-Lipid Nanoparticle COVID-19 Vaccines: Structure and Stability. Int. J. Pharm 2021, 601, 120586. [PubMed: 33839230]

(27). Zhang L; Yi H; Song J; Huang J; Yang K; Tan B; Wang D; Yang N; Wang Z; Li X Mitochondria-Targeted and Ultrasound-Activated Nanodroplets for Enhanced Deep-Penetration Sonodynamic Cancer Therapy. ACS Appl. Mater. Interfaces 2019, 11, 9355–9366. [PubMed: 30734551]

(28). Wang W; Jiang S; Li S; Yan X; Liu S; Mao X; Yu X Functional Choline Phosphate Lipids for Enhanced Drug Delivery in Cancer Therapy. Chem. Mater 2021, 33, 774–781.

(29). Wang J; Liu G Imaging Nano-Bio Interactions in the Kidney: Toward a Better Understanding of Nanoparticle Clearance. Nanomaterials and Neoplasms 2021, 57, 847–854.

(30). Tsoi KM; MacParland SA; Ma X-Z; Spetzler VN; Echeverri J; Ouyang B; Fadel SM; Sykes EA; Goldaracena N; Kaths JM; Conneely JB; Alman BA; Selzner M; Ostrowski MA; Adeyi OA; Zilman A; McGilvray ID; Chan WCW Mechanism of Hard-Nanomaterial Clearance by the Liver. Nat. Mater 2016, 15, 1212–1221. [PubMed: 27525571]

(31). Baker KG; Robertson VJ; Duck FA A Review of Therapeutic Ultrasound: Biophysical Effects. Physical Therapy 2001, 81, 1351–1358. [PubMed: 11444998]

(32). Meng Y; Hynynen K; Lipsman N Applications of Focused Ultrasound in the Brain: From Thermoablation to Drug Delivery. Nat. Rev. Neurol 2021, 17, 7–22. [PubMed: 33106619]

(33). Chang N; Qin D; Wu P; Xu S; Wang S; Wan M IR780 Loaded Perfluorohexane Nanodroplets for Efficient Sonodynamic Effect Induced by Short-Pulsed Focused Ultrasound. Ultrason. Sonochem 2019, 53, 59–67. [PubMed: 30559082]

(34). Li WP; Su CH; Chang YC; Lin YJ; Yeh CS Ultrasound-Induced Reactive Oxygen Species Mediated Therapy and Imaging Using a Fenton Reaction Activable Polymersome. ACS Nano 2016, 10, 2017–2027. [PubMed: 26720714]

(35). Gomes A; Fernandes E; Lima JLFC Fluorescence Probes Used for Detection of Reactive Oxygen Species. J. Biochem. Biophys. Methods 2005, 65, 45–80. [PubMed: 16297980]

(36). Wang W; Lin L; Ma X; Wang B; Liu S; Yan X; Li S; Tian H; Yu X Light-Induced Hypoxia-Triggered Living Nanocarriers for Synergistic Cancer Therapy. ACS Appl. Mater. Interfaces 2018, 10, 19398–19407. [PubMed: 29781276]

(37). Entradas T; Waldron S; Volk M The Detection Sensitivity of Commonly Used Singlet Oxygen Probes in Aqueous Environments. J. Photochem. Photobiol. B 2020, 204, 111787. [PubMed: 31958676]

(38). Wang J; Yi J Cancer Cell Killing via ROS: To Increase or Decrease, That Is the Question. Cancer Biol. Ther 2008, 7, 1875–1884. [PubMed: 18981733]

(39). Mittler RROSA ROS Are Good. Trends Plant Sci. 2017, 22, 11–19. [PubMed: 27666517]

(40). Zhang F; Wang L-P; Brauner M; Liewald JF; Kay K; Watzke N; Wood PG; Bamberg E; Nagel G; Gottschalk A; Deisseroth K Multimodal Fast Optical Interrogation of Neural Circuitry. Nature 2007, 446, 633–639. [PubMed: 17410168]

(41). Holt RG; Roy RA Measurements of Bubble-Enhanced Heating from Focused, MHz-Frequency Ultrasound in a Tissue-Mimicking Material. Ultrasound Med. Biol 2001, 27, 1399–1412. [PubMed: 11731053]

(42). Hochbaum DR; Zhao Y; Farhi SL; Klapoetke N; Werley CA; Kapoor V; Zou P; Kralj JM; Maclaurin D; Smedemark-Margulies N; Saulnier JL; Boulting GL; Straub C; Cho YK; Melkonian M; Wong GK-S; Harrison DJ; Murthy VN; Sabatini BL; Boyden ES; Campbell RE; Cohen AE All-Optical Electrophysiology in Mammalian Neurons Using Engineered Microbial Rhodopsins. Nat. Methods 2014, 11, 825–833. [PubMed: 24952910]

(43). Dobrovolskaia MA; Clogston JD; Neun BW; Hall JB; Patri AK; McNeil SE Method for Analysis of Nanoparticle Hemolytic Properties in Vitro. Nano Lett. 2008, 8, 2180–2187. [PubMed: 18605701]

(44). Amin K; Dannenfelser R-M Vitro Hemolysis: Guidance for the Pharmaceutical Scientist. J. Pharm. Sci 2006, 95, 1173–1176. [PubMed: 16639718]

(45). Sanes JN; Donoghue JP Plasticity and Primary Motor Cortex. Annu. Rev. Neurosci 2000, 23, 393–415. [PubMed: 10845069]

(46). Sato T; Shapiro MG; Tsao DY Ultrasonic Neuromodulation Causes Widespread Cortical Activation via an Indirect Auditory Mechanism. Neuron 2018, 98, 1031–1041 e5. [PubMed: 29804920]

(47). Blackmore J; Shrivastava S; Sallet J; Butler CR; Cleveland RO Ultrasound Neuromodulation: A Review of Results, Mechanisms and Safety. Ultrasound Med. Biol 2019, 45, 1509–1536. [PubMed: 31109842]

(48). Yu K; Niu X; Krook-Magnuson E; He B Intrinsic Functional Neuron-Type Selectivity of Transcranial Focused Ultrasound Neuromodulation. Nat. Commun 2021, 12, 2519. [PubMed: 33947867]

(49). Arenkiel BR; Peca J; Davison IG; Feliciano C; Deisseroth K; Augustine GJ; Ehlers MD; Feng G Vivo Light-Induced Activation of Neural Circuitry in Transgenic Mice Expressing Channelrhodopsin-2. Neuron 2007, 54, 205–218. [PubMed: 17442243]

(50). Zhao S; Ting JT; Atallah HE; Qiu L; Tan J; Gloss B; Augustine GJ; Deisseroth K; Luo M; Graybiel AM; Feng G Cell Type–specific Channelrhodopsin-2 Transgenic Mice for Optogenetic Dissection of Neural Circuitry Function. Nat. Methods 2011, 8, 745–752. [PubMed: 21985008]

(51). Pinto L; Goard MJ; Estandian D; Xu M; Kwan AC; Lee S-H; Harrison TC; Feng G; Dan Y Fast Modulation of Visual Perception by Basal Forebrain Cholinergic Neurons. Nat. Neurosci 2013, 16, 1857–1863. [PubMed: 24162654]

(52). Thyagarajan S; van Wyk M; Lehmann K; Lowel S; Feng G; Wassle H Visual Function in Mice with Photoreceptor Degeneration and Transgenic Expression of Channelrhodopsin 2 in Ganglion Cells. J. Neurosci 2010, 30, 8745–8758. [PubMed: 20592196]

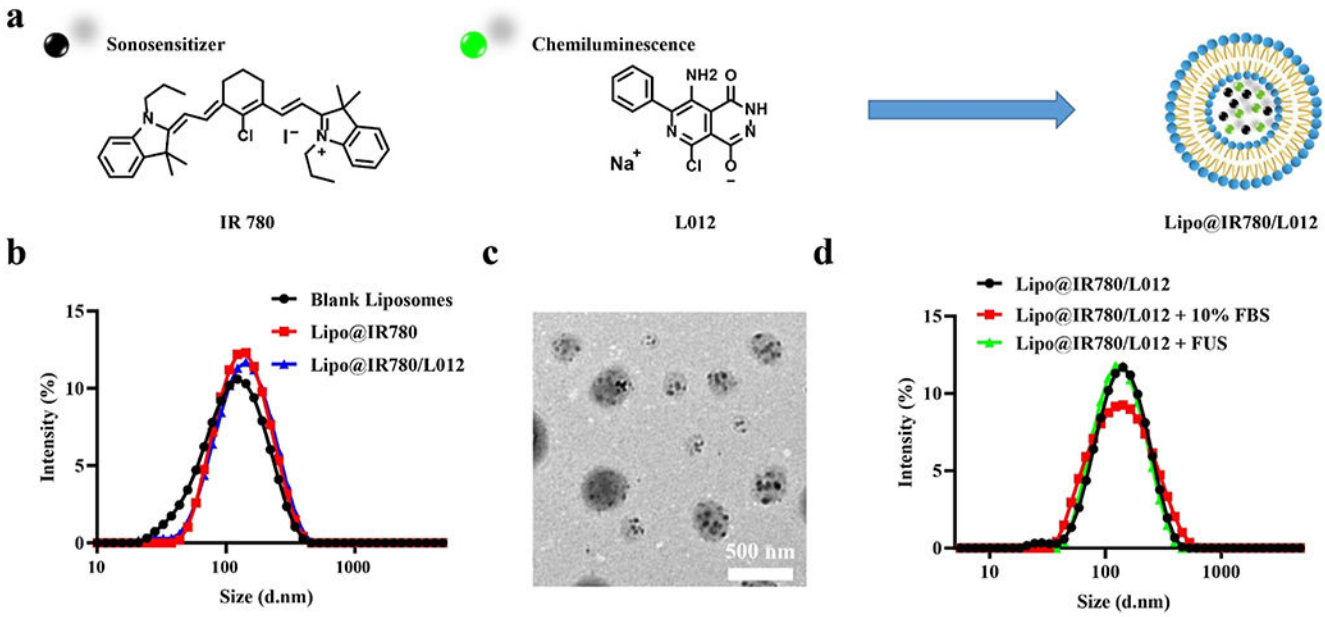

Figure 1.

Nano performance of Lipo@IR780/L012. (a) Illustration of the IR780-and L012-loaded liposome, Lipo@IR780/L012; (b) size distribution of the blank liposome, Lipo@IR780, and Lipo@IR780/L012 determined via DLS; (c) TEM image of Lipo@IR780/L012; and (d) size stability tests of Lipo@IR780/L012 with/without 10% FBS or under the FUS irradiation, determined by DLS.

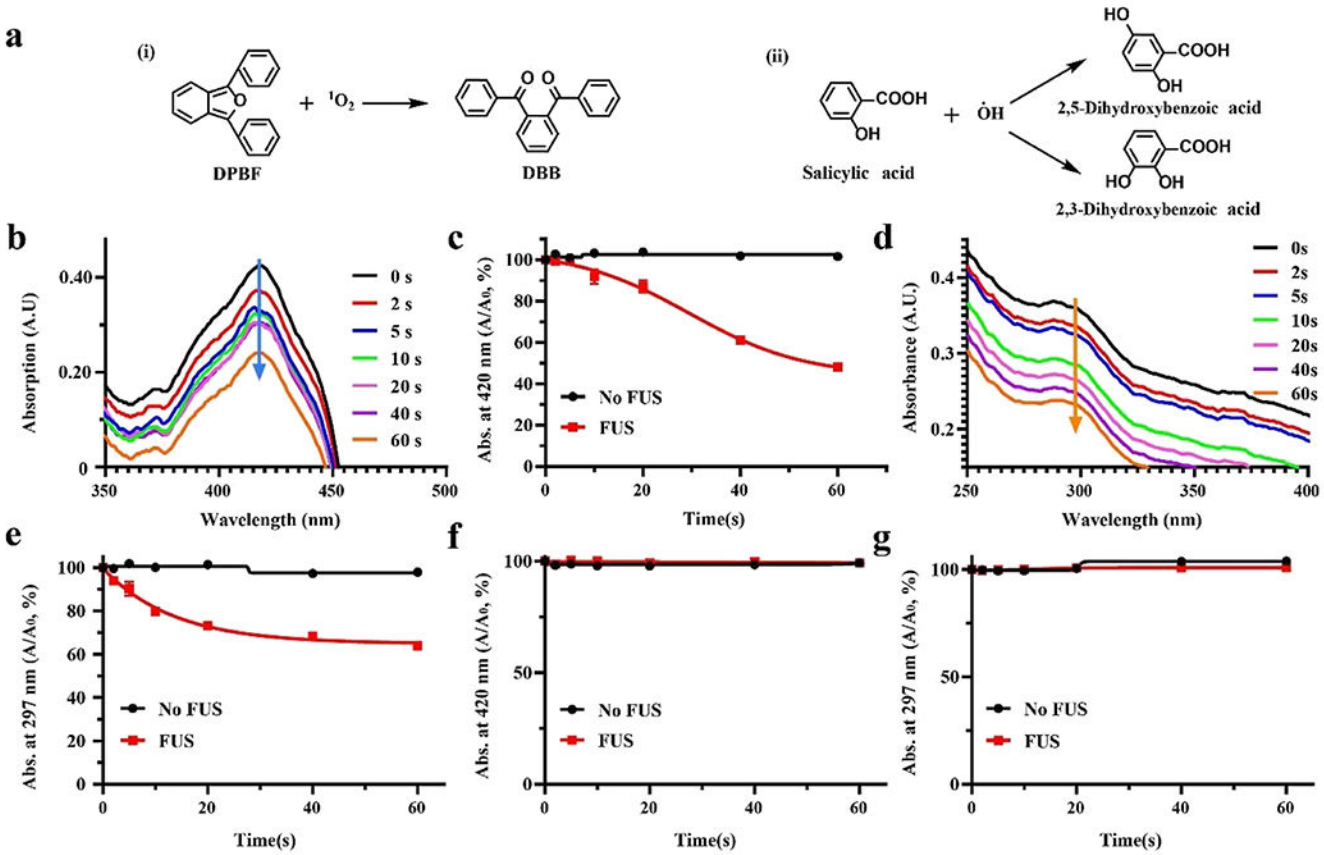

Figure 2.

FUS-induced ROS generation of Lipo@IR780 nanoparticles. (a) Reaction mechanism of ROS probes in the presence of ROS, (i) DPBF specifically reacts with $^1O_2$ to generate DBB, (ii) SA will react in the presence of ·OH to generate dihydroxybenzoic acid; (b) time-dependent UV–vis degradation spectrum of DPBF indicating that $^1O_2$ was generated via Lipo@IR780 under FUS (1.5 MHz, peak pressure 1.5 MPa); (c) quantification analysis of DPBF decomposition in the presence of Lipo@IR780 with and without FUS irradiation ($n > 3$ per group); (d) time-dependent UV–vis degradation spectrum of SA indicating that ·OH was generated via Lipo@IR780 under FUS (1.5 MHz, peak pressure 1.5 MPa) ($n > 3$ per group); (e) quantification analysis of SA decomposition in the presence of Lipo@IR780 with and without FUS irradiation ($n > 3$ per group); (f) quantification analysis of DPBF decomposition in the presence of Lipo@IR780/L012 with and without FUS irradiation ($n > 3$ per group), indicating that no $^1O_2$ residues escaped from liposomes; and (g) quantification analysis of SA decomposition in the presence of Lipo@IR780/L012 with and without FUS irradiation ($n > 3$ per group), indicating that no ·OH residues escaped from liposomes. All plots show mean ± SEM unless otherwise mentioned.

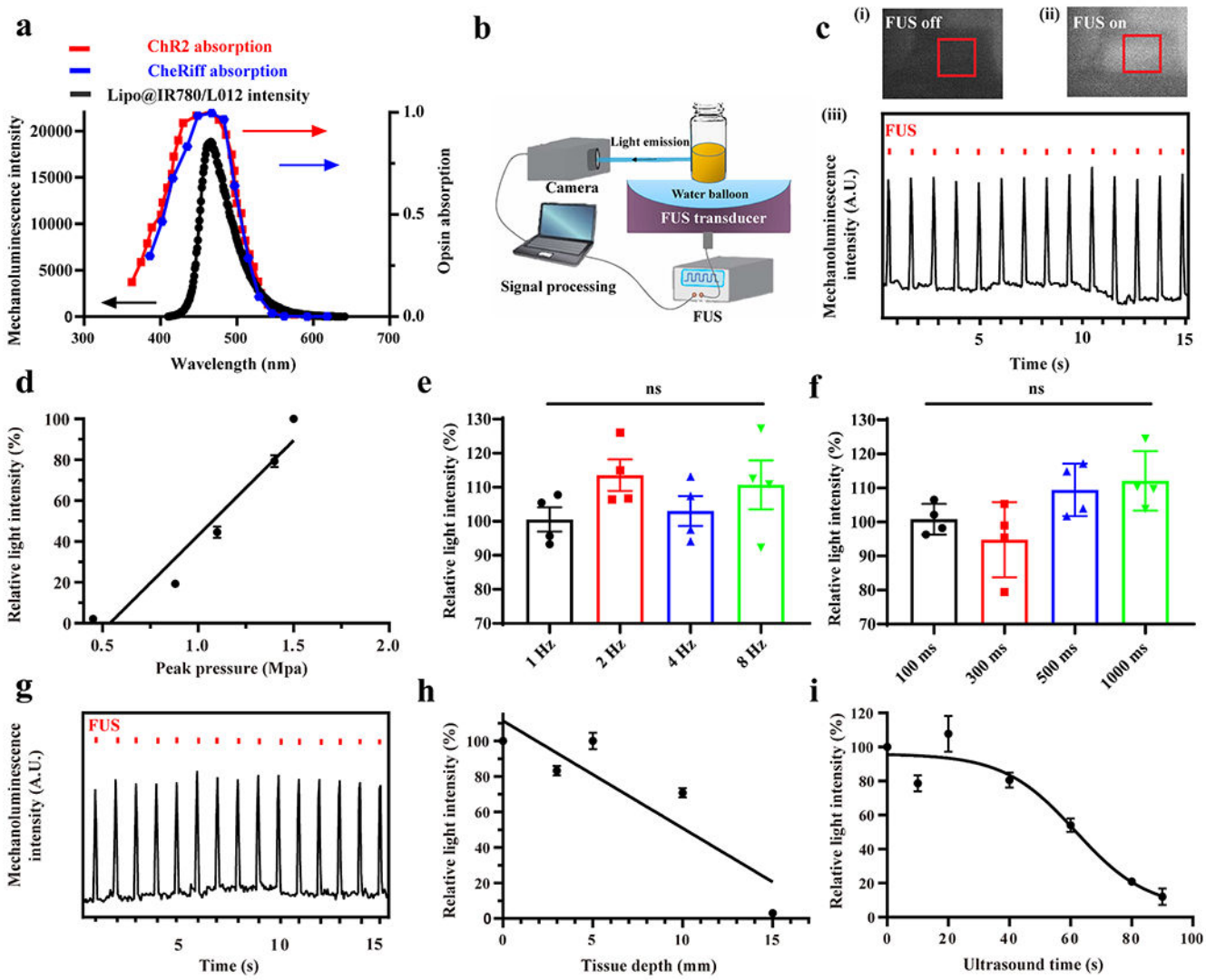

Figure 3.

FUS-triggered light emission of Lipo@IR780/L012. (a) Mechanoluminescence spectrum of Lipo@IR780/L012 nanoparticles (black) overlaid with the ChR2 absorption spectrum (red dotted curve) and CheRiff absorption spectrum (blue dotted curve); (b) illustration of the FUS-induced light emission of Lipo@IR780/L012 nanoparticles and signal processing; (c) blue light was generated from Lipo@IR780/L012 nanoparticles under FUS irradiation (1.5 MHz, pulse 100 ms on, 900 ms off, 1 Hz, 1.5 MPa): photography of Lipo@IR780/L012 nanoparticles when the FUS was (i) off and (ii) on and (iii) 470 nm blue light emission from Lipo@IR780/L012 nanoparticles under the repetitive FUS irradiation; (d) quantification analysis of light density indicating that the light emission of Lipo@IR780/L012 nanoparticles increases linearly with FUS peak pressure; (e) Lipo@IR780/L012 nanoparticles light emission intensity under different FUS irradiation frequencies [$n = 4$ per group, one-way analysis of variance (ANOVA)] (1.5 MHz, 1.5 MPa); (f) Lipo@IR780/L012 nanoparticles light emission intensity under different pulse intervals ($n = 4$ per group, one-way ANOVA) (1.5 MHz, 1.5 MPa); (g) blue light emission from Lipo@IR780/L012

nanoparticles upon FUS irradiation under 10 mm pork skin (1.5 MHz, pulse 100 ms on, 900 ms off, 1 Hz, 1.5 MPa); (h) quantification analysis of light density at different pork skin depths (1.5 MHz, pulse 100 ms on, 900 ms off, 1 Hz, 1.5 MPa) under FUS irradiation; and (i) light density of Lipo@IR780/L012 nanoparticles decayed with continuous FUS irradiation. All plots show mean ± SEM unless otherwise mentioned. *$P < 0.05$, **$P < 0.01$, ***$P < 0.001$, and ****$P < 0.0001$; ns, not significant.

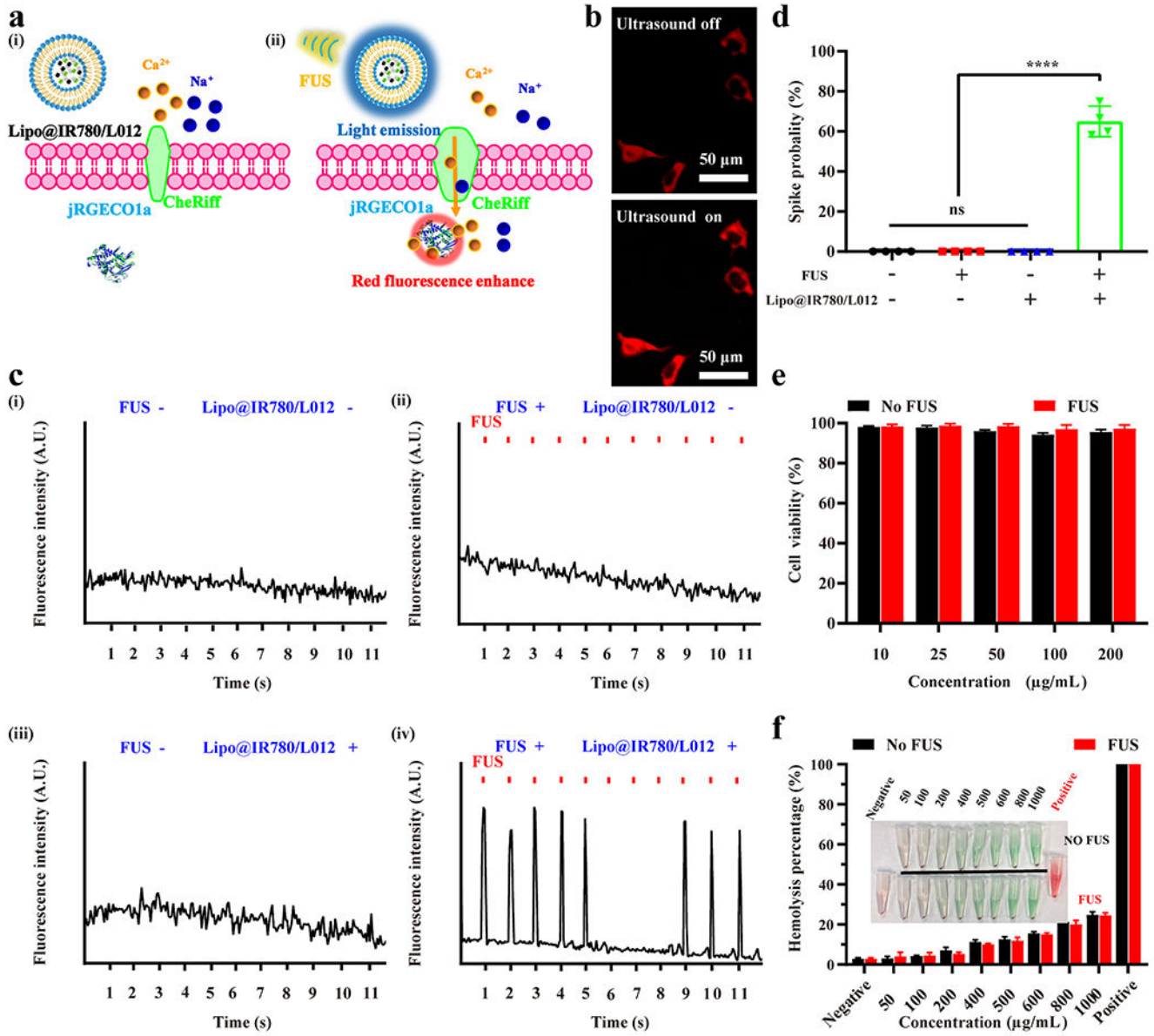

Figure 4.

In vitro sono-optogenetic stimulation and biosafety tests of Lipo@IR780/L012. (a) Illustration of FUS-triggered CheRiff channels opening due to 470 nm blue light emission from Lipo@IR780/L012 nanoparticles. The flow of Ca^{2+} into the cells binds with jREGCO1a proteins to enhance the red fluorescence signal. (b) Fluorescence images of CheRiff-expressing spiking HEK cells with and without mechanoluminescence irradiation from Lipo@IR780/L012 nanoparticles: ultrasound off and ultrasound on; (c) fluorescence signal recording from CheRif-expressing spiking HEK cells under the following conditions: (i) no FUS and no Lipo@IR780/L012 nanoparticles; (ii) with FUS (1.5 MHz, puls 100 ms on, 900 ms off, 1 Hz, 1.5 MPa) and no Lipo@IR780/L012 nanoparticles; (iii) no FUS and with Lipo@IR780/L012 nanoparticles; (iv) with FUS (1.5 MHz, puls 100 ms on, 900 ms off, 1 Hz, 1.5 MPa) and with Lipo@IR780/L012 nanoparticles; and (d) spike probability of

CheRiff-expressing spiking HEK cells under the different conditions ($n = 4$ per group, two-way ANOVA). (e) Cell viability tests of Lipo@IR780/L012 nanoparticles in HEK cells with and without FUS irradiation (n = 5 per group). (f) Hemolysis tests of Lipo@IR780/L012 nanoparticles ($n = 3$ per group). All plots show mean ± SEM unless otherwise mentioned. *$P < 0.05$, **$P < 0.01$, ***$P < 0.001$, and ****$P < 0.0001$; ns, not significant.

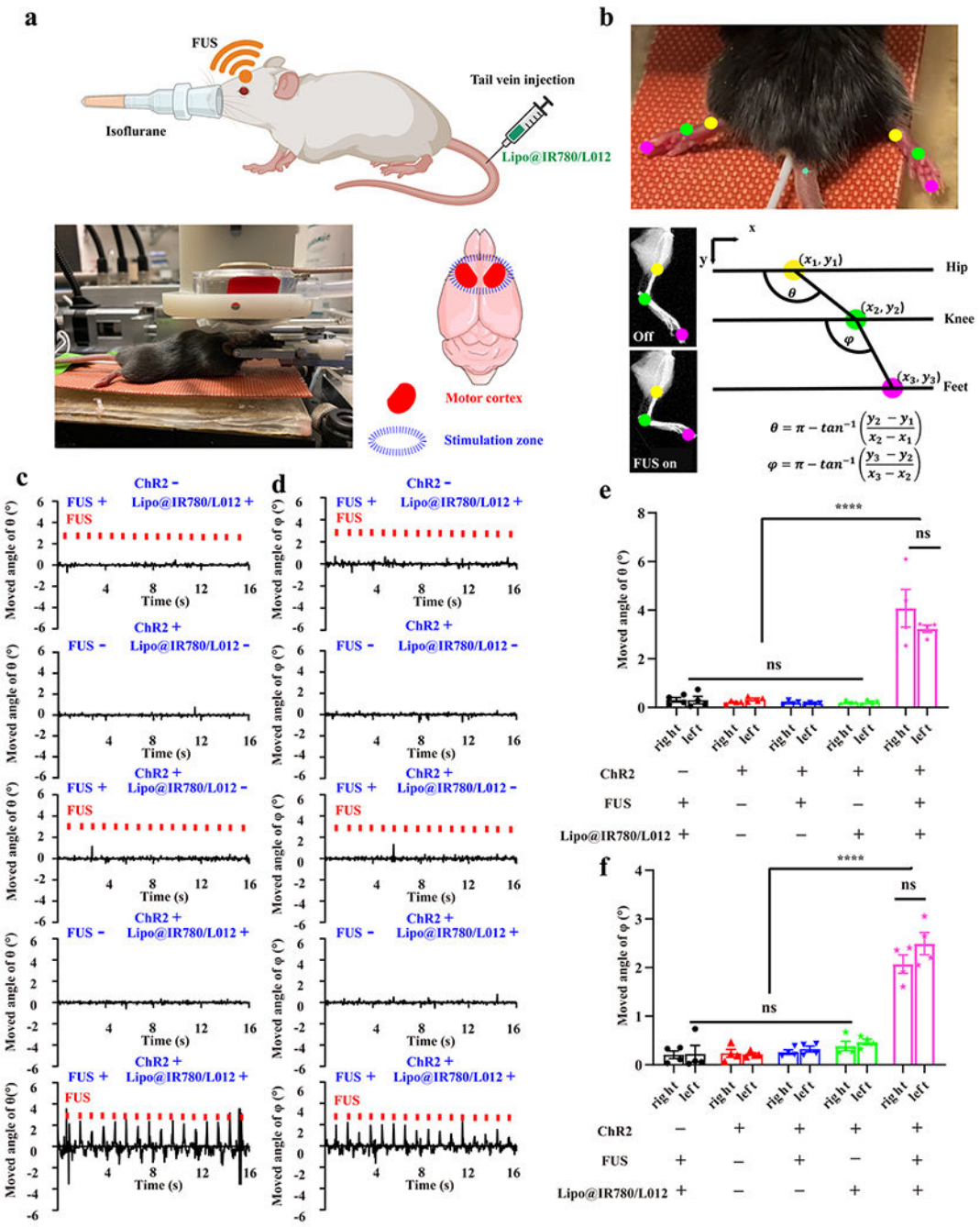

Figure 5.

In vivo sono-optogenetic motor cortex stimulation. (a) Schematic of in vivo noninvasive sono-optogenetic brain stimulation, where the mouse was fixed in a stereotaxic frame and deeply anesthetized using 2.5% isoflurane, and then, Lipo@IR780/L012 nanoparticles were injected through the tail vein. The FUS transducer was in direct contact with the scalp of the mouse during brain stimulation, where the photograph of the in vivo sono-optogenetics is given. The motor cortex zone was irradiated via FUS, created using BioRender.com. (b) Limbs' response to FUS was recorded via a camera and analyzed via DeepLabCut. The

photograph of limbs' response to FUS was used to track the brain activation, where different colored dots were marked on joints to track the movement, and kinematic joint angle changes of hip–knee (θ) and knee–feet (φ) response to FUS were tracked and calculated through DeepLabCut. (c) Time-resolved right limb's hip–knee response and (d) knee–feet response to FUS, including no FUS and no Lipo@IR780/L012 nanoparticles, with FUS (1.5 MHz, puls 100 ms on, 900 ms off, 1 Hz, 2.2 MPa) but no Lipo@IR780/L012 nanoparticles, no FUS with Lipo@IR780/L012 nanoparticles, and with both FUS (1.5 MHz, puls 100 ms on, 900 ms off, 1 Hz, 2.2 MPa) and Lipo@IR780/L012 nanoparticles in Thy1-ChR2-YFP transgenic mice and C57BL/6J wild type mice with Lipo@IR780/L012 and FUS. (e) Statistical analysis of the hip–knee and (f) knee–feet angle changes in different groups of subjects ($n = 4$ per group, two-way ANOVA) in response to FUS irradiation. All plots show mean ± SEM unless otherwise mentioned. $^{*}P < 0.05$, $^{**}P < 0.01$, $^{***}P < 0.001$, and $^{****}P < 0.0001$; ns, not significant.

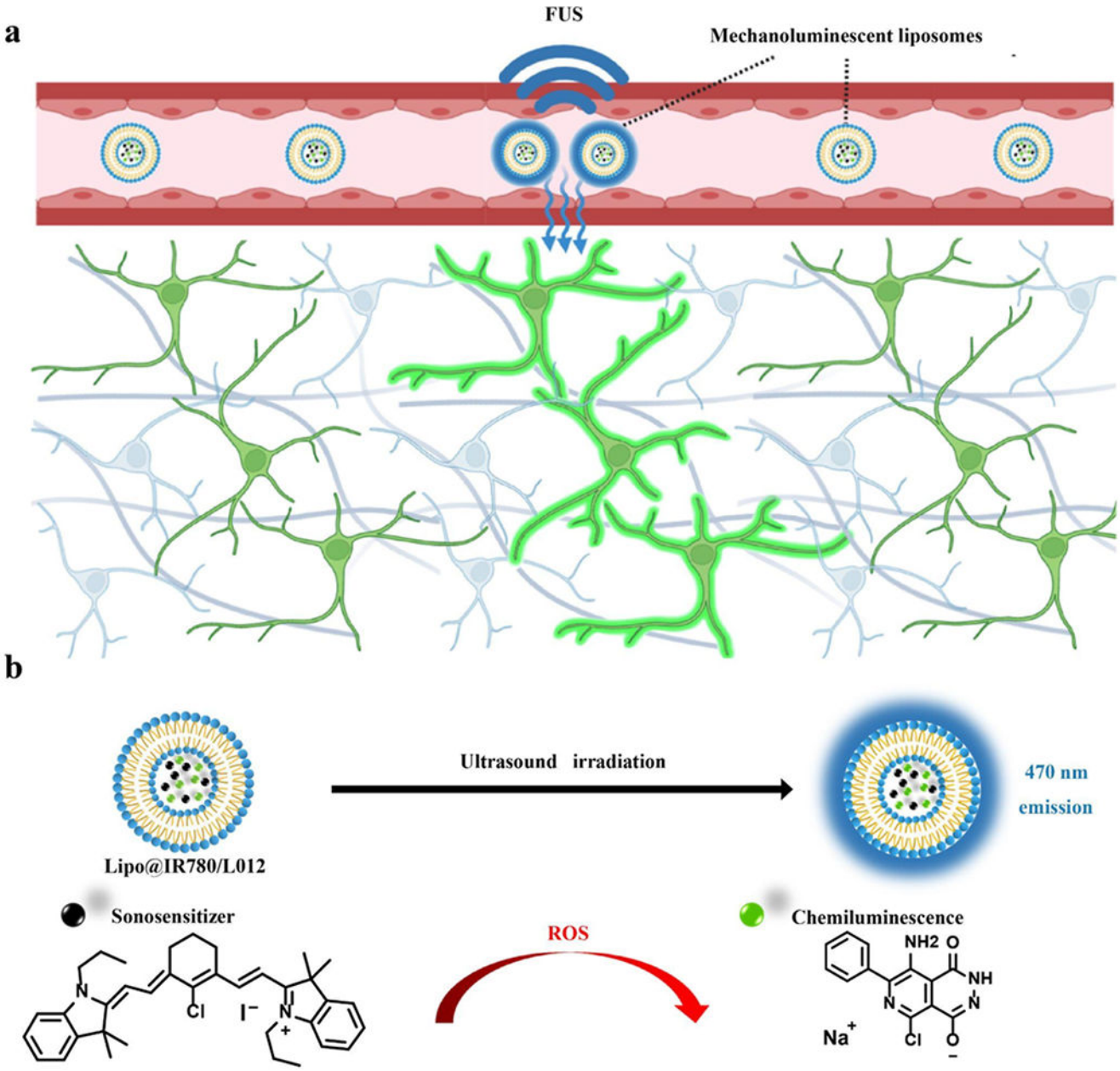

Scheme 1. Schematic of FUS-Triggered Blue Light Emission From Lipo@IR780/L012[a]

[a](a) After i.v. injection, Lipo@IR780/L012 nanoparticles circulate in blood and emit blue light to the surrounding for optogenetic stimulation of opsin-expressing neurons under FUS irradiation; the diagram is created using Biorender.com. (b) Mechanism of light emission of Lipo@IR780/L012 nanoparticles under FUS irradiation.

Table 1.

Details of Various Liposomes Determined via DLS and UV–Vis Spectroscopy

entries	Nanoparticles	Size (*d* nm)	PDI	Zeta potential (mv)	DLC (wt %) of IR780	DLC (wt %) of L012
1	Blank Lipo	105.0 ± 3.7	0.228	−28.0 ± 1.3	N/A	N/A
2	Lipo@IR780	119.3 ± 0.2	0.183	−24.1 ± 0.5	4.63 ± 0.59	N/A
3	Lipo@IR780/L012	120.9 ± 0.5	0.189	−25.8 ± 0.7	4.61 ± 0.66	4.30 ± 0.44
4	Lipo@IR780/L012 + 10% FBS	119.7 ± 0.8	0.196	N/A	N/A	N/A
5	Lipo@IR780/L012 + FUS	120.2 ± 0.2	0.188	N/A	N/A	N/A